water

MDPI

Article

Turbulent Flow Structures in Developing and Fully-Developed Flows under the Impact of Downward Seepage

Anurag Sharma [1], Bimlesh Kumar [2,*] and Giuseppe Oliveto [3]

[1] Department of Civil Engineering, National Institute of Technology Rourkela, Rourkela 769008, India; sharmaan@nitrkl.ac.in
[2] Department of Civil Engineering, Indian Institute of Technology Guwahati, Guwahati 781039, India
[3] School of Engineering, University of Basilicata, Viale dell'Ateneo Lucano 10, 85100 Potenza, Italy; giuseppe.oliveto@unibas.it
* Correspondence: bimk@iitg.ac.in

Abstract: This work experimentally investigates the turbulent flow characteristics of developing and fully-developed flows over a rough bed channel that is subjected to downward seepage. Instantaneous 3D velocities were collected using an acoustic Doppler velocimeter (ADV) in the developing and fully-developed flow regions, along the channel centerline, to analyze different turbulent statistics. Observations revealed that the streamwise and vertical velocities were higher in developing flows, whereas the Reynolds shear stresses, and turbulence intensities, were smaller. The downward seepage would affect the velocity distributions and flow depth in both the developing and fully-developed regions. Therefore, new equations to represent the distribution of the turbulence intensities were proposed, and a comparison with the current literature is provided. The investigation of the Reynolds stress anisotropy tensors concludes that the degree of anisotropy in fully-developed flows is lower than for developing flows.

Keywords: developing flow; fully-developed flow; Reynolds stress anisotropy tensor; seepage flow; turbulence intensity

Citation: Sharma, A.; Kumar, B.; Oliveto, G. Turbulent Flow Structures in Developing and Fully-Developed Flows under the Impact of Downward Seepage. *Water* **2022**, *14*, 500. https://doi.org/10.3390/w14030500

Academic Editors: Vlassios Hrissanthou and Giuseppe Pezzinga

Received: 22 November 2021
Accepted: 4 February 2022
Published: 8 February 2022

1. Introduction

The flow in open channels is mainly turbulent in nature. In general, open-channel flows are spatially varied in the field due to the frequent variations of the boundary conditions arising from the alterations in flow discharge, as well as other channel parameters [1]. The alterations in boundary conditions cause a flow disruption due to the variance of viscous, gravitational, and inertial forces. Eventually, the flow attempts to reach a fully-developed flow condition in the downstream course. At the channel entrance, a high-velocity gradient is developed close to the channel boundary that is linked with the frictional stresses developed between the fluid particles and the rough surface [2]. The fluid layer close to a rough surface, where viscous properties are apparent, is termed the boundary layer. The boundary layer may be laminar at the inlet section of the channel and gradually thickens up to a definite distance along the channel length, where the flow is termed as developing flow; behind the developing length, the flow becomes a fully-developed flow [3]. For rough boundaries, the viscous properties can be observed in a very thin layer, termed the viscous sublayer, in which the major portion of the velocity variation arises. In fully-developed turbulent flow, with respect to the velocity governing factors, the boundary layer is formed from the inner zone and the outer zone. The inner zone is again composed by the viscous sublayer and the fully turbulent inner region. It is important to investigate the fluid features in developing and developed open-channel flows to evaluate the fluid–sediment interface and sediment aggradation and degradation, which are closely related to the hydrodynamic features, such as the vertical profile of time-averaged velocities, turbulence intensities, Reynolds shear stresses, and turbulent kinetic energy [1]. The

turbulent developing open-channel flow is a complex 3D flow governed by a seepage bed, the bed roughness, and other variables.

The two-component flow time-averaged velocity profile in open channels is fundamental in studying bed shear stresses and the occurrence of bed material transport [3–6]. Studies from the literature indicate that the standard log-law is valid for the longitudinal velocity depth profiles in the inner layer of the flow, which is 0.2 times the flow depth above the boundary wall [7,8]. These studies highlight that the log-law diverges from the observed data for the outer layer of flow and is replaced by the wake-law [9]. Kirkgöz and Ardiçlioğlu [2] showed that, in developed flows in wide-open-channels, the flow velocity achieves its maximum value close to the water surface. Mahananda et al. [10] experimentally investigated the turbulence characteristics in developing and fully-developed flows in narrow open-channel flow over a rough bed. They proposed an analytical power law for the time-averaged velocity distribution and matched it with the observed velocity. Besides the laboratory observations, numerous analytical results have also projected the velocity profile in fully-developed flows [11].

There are several studies [4–11] on the turbulence characteristics for fully-developed flows in open channels. On the contrary, the turbulent flow structures in developing flows in open channels are not sufficiently addressed; this is even more evident when seepage conditions also occur. The flow turbulence in the developing zone of an open channel is a three-dimensional flow affected by a downward seepage flow. Studying turbulent features of flow in the developing zone of a channel over a rough bed, which is frequently experienced in fluvial hydraulics, is, therefore, of importance. Marusic et al. [12] specified that a developed flow is the flow in which turbulent parameters and the hydraulic parameters are free from the longitudinal distance towards the flow development. Seepage is a process that influences the turbulent characteristics of the flow and the bed material movement at the bed surface [13,14]. As a practical example, the dynamics of turbulence and seepage govern a significant feature of the transport of solutes through the hyporheic river zone [15], which has important implications for groundwater quality. Field studies [16,17] calculated the quantity of downward seepage in an alluvial river and revealed that the amount of seepage might lie between 10% and 45% of the channel discharge supplied at the canal head. This paper aimed to emphasize the eventual differences between the turbulent flow structures for developing and fully-developed flows in sandy-bed straight channels, considering downward seepage processes. Specifically, the distributions along the flow depth of the streamwise and vertical velocities, turbulence intensities, and Reynolds shear stresses were analyzed. Moreover, the turbulent correlation coefficient, the turbulent kinetic energy (TKE), and the Reynolds stress anisotropy tensor were considered for a deeper exploration.

2. Experimental Methodology

Experiments were conducted in a 17.2 m long, 1.00 m wide, and 0.72 m deep glass-walled rectangular flume in the Water Resources Engineering Laboratory at the Indian Institute of Technology, Guwahati, India. The bed slope of the flume was kept constant for the no-seepage and seepage runs with a value of 0.0005 (Figure 1). A couple of baffle walls were fixed at the inlet of the flume to decrease the degree of flow turbulence when the water entered the channel. The bed was levelled with glass with a smooth finish, and was made with a non-uniform sediment with a median grain size of d_{50} = 0.5 mm and geometric standard deviation of σ_g $(d_{84.1} - d_{15.9})/d_{50}$ = 1.65 to achieve a rough bed surface. It should be noted that $d_{84.1}$, $d_{15.9}$, and d_{50} represented the size of the particles for which the percentage of finer particles were 84.1, 15.9, and 50, respectively. Water was recirculated between the underground trench and the channel by using two centrifugal pumps. The tailgate was adjusted for the required flow depth in the channel. A valve positioned at the upper section of the inlet tank allowed for the preselected flow discharge. Further experimental details are available in Sharma and Kumar [14]. The channel bed was prepared with a non-porous section 2 m from the upstream end of the channel, and the remaining length (15.2 m) was prepared with a porous section by covering it in a fine mesh

(0.1 mm). The fine mesh was sustained by the steel tube arrangement that was 0.22 m high, which was positioned on the bottom of the flume. The experimental setup for downward seepage was prepared by creating a seepage chamber 15.20 m long, 1.0 m wide, and 0.22 m deep. The seepage chamber was located beneath the flume bed to collect the loss of water from the downward seepage. The non-uniform sediment mixture was placed on a fine mesh that was 0.1 mm squared to ensure the free flow conditions from the entry to the seepage zone. The quantity of the seepage discharge was controlled with a pair of valves fixed to the seepage chamber at the outlet end of the flume by forming a pressure difference between the seepage chamber and the channel. The seepage was approximately uniform (slightly non-uniform), and was applied throughout the seepage zone length in order to maintain a constant seepage discharge in the main channel along the streamwise direction. Two electromagnetic flowmeters (EFMs), with an accuracy of $\pm$ 0.5%, were attached to the seepage chamber (pressure chamber) through pipes, which were utilized to measure the desired quantity of the seepage discharge [14]. The uncertainty associated with the experimental data was calculated before performing the experiments. The uncertainty regarding the measurements of the seepage discharge from the electromagnetic flowmeter was analyzed using various repeated tests. The standard uncertainty for the seepage discharge was approximately 3.75%, which suggests a satisfactory accuracy of the EFM used for the discharge measurement. Regarding the coordinate system of the channel, the streamwise velocity component was along the x-axis, the lateral velocity component was along the y-axis, and the vertical velocity component was along the z-axis, which was in a positive direction, upward from the bed surface. The flow depth was measured with a digital point gauge attached to a Vernier scale.

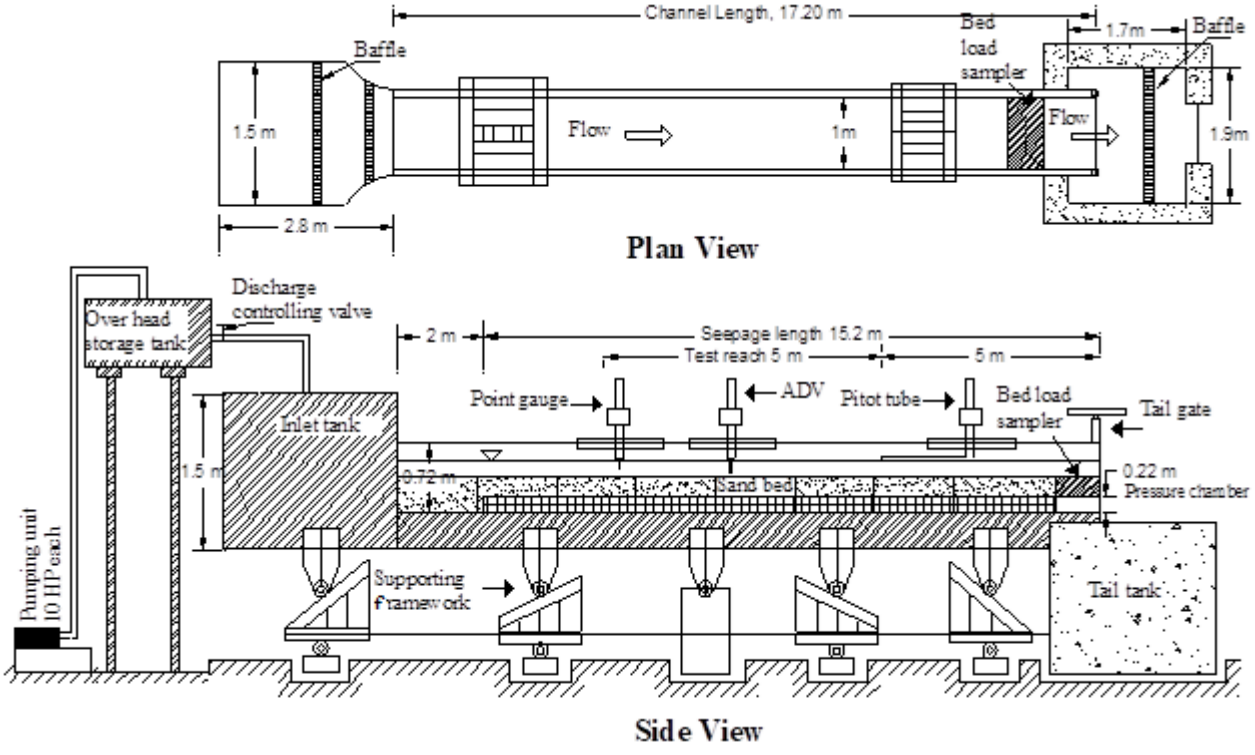

Figure 1. Schematic of experimental setup.

A four-beam down-looking acoustic Doppler velocimeter (VectrinoPlus) was used to measure the three-dimensional instantaneous water velocities. By analyzing the velocity distributions taken along the centerline at every 100 cm, the flow region was observed, fully-developed, when $x \geq 5$ m, consistent with the results of previous studies [3]. Therefore, the velocity data sets were collected at the centerline of the channel cross-section. The data were recorded at various distances from the upstream end of the channel (x = 3 and 7 m) to

compare the turbulent flow structures in the developing and fully-developed flows. The nearest measuring point of velocity was taken at a distance of 1–2 mm from the bed surface, and the velocity measurement farthest from the bed was taken 50 mm beneath the water surface. In the vicinity of the bed surface, the velocities were measured with an interval of 1–2 mm, while near the free surface, they were achieved with an interval of 4–5 mm. The instantaneous velocities were measured by ADV at a position 50 mm beneath the probe emitter to reduce the effect of the probe on the experimental data. The data acquisition sampling frequency was 200 Hz. The sampling volume was a 1 to 4 mm long cylinder with a diameter of 6 mm. For the velocity data collection in the flow's outer layer, the sampling volume was maintained at 4 mm long. In the vicinity of channel boundary, the length of the sampling volume was changed to 1 mm so that it did not collide with the sediment particles on the bed. The sampling length of 1 mm was adequate to achieve the real velocity distributions close to the channel bed. The signal-to-noise ratio and the correlation magnitude were higher than 10 and 60, respectively. The instantaneous ADV data were collected for the sampling duration of 300 s. The spikes present in the ADV velocity data were removed by a modified singular spectrum technique, as suggested by Sharma et al. [18].

Two experimental runs were carried out with a flow discharge of Q = 0.0402 m^3/s and seepage discharge of Q_s = 0.00402 m^3/s (Q_s = 10% of the flow discharge). The heights of water for the no-seepage and seepage experiments were 0.116 m and 0.112 m, respectively. The velocity measurements were taken at the developing flow region (x = 3 m from the inlet) and the fully-developed flow region (x = 7 m from the inlet) for the no seepage and downward seepage conditions. These four experimental data sets were recorded as E1 to E4. The experiments E1 and E2 represent the developing and fully-developed flow conditions in the case of the no seepage bed condition. Similarly, the experiments E3 and E4 represent the developing and developed flow in the case of the downward seepage condition. In all experimental runs, the aspect ratio was greater than five [19], ensuring negligible wall effects.

More experimental details are provided in Table 1, with Re, Fr, h, and U representing the flow Reynolds numbers ($Re = Uh/v$, where v is the kinematic viscosity), the flow Froude number $Fr = U/\sqrt{gh}$, the flow depth, and the depth-averaged flow velocity in the developed region of the open-channel flow, respectively.

Table 1. Main hydraulic parameters for the experimental runs of this study.

	h (m)	Q (m^3/s)	Re	U (m/s)	Fr	Q_S (m^3/s)	Experimental Run
No seepage	0.116	0.0402	32,630	0.346	0.3248	0	**E1** (Developing flow) **E2** (Developed flow)
10% seepage	0.112	0.0402	32,850	0.359	0.3424	0.00402	**E3** (Developing flow) **E4** (Developed flow)

3. Results and Discussion

In the present paper, u, v, and w represent the mean streamwise, lateral, and vertical velocity components, respectively, while u', v', and w' are the fluctuating components of the velocities, respectively. Similarly, $\left(\overline{u'u'}\right)^{0.5}$, $(\overline{v'v'})^{0.5}$ and $(\overline{w'w'})^{0.5}$ are the turbulence intensities. Moreover, u_* [$=(\tau_0/\rho)^{0.5}$] represents the shear velocity where τ_0 = the boundary shear stress observed from the distribution of the Reynolds shear stresses (τ_{uw}) projected to the bed surface, which is $\tau_0 = (\tau_{uw})_{z=0}$ as given by Nezu and Nakagawa [20]. The shear velocity for the experimental datasets E1, E2, E3, and E4 were 14.41 mm/s, 14.57 mm/s, 14.65 mm/s, and 15.02 mm/s, respectively. In the near-bed zone, the uncertainty errors for the velocities and the Reynolds shear stresses were lower than 5% and 12.5%, respectively, indicating ADV data accuracy. Moreover, based on the flow field classification suggested by Nezu and Nakagawa [20], the present study distinguished the flow field into four layers: (i) the inner layer ($z/h < 0.2$); (ii) the outer layer ($z/h \geq 0.2$); (iii) the intermediate layer

($0.2 \leq z/h \leq 0.6$), and (iv) the free surface layer ($0.6 < z/h \leq 1$). This categorization of the flow field was used to examine the key profiles of the fluid features.

3.1. Time-Averaged Velocities

Figure 2 shows the streamwise and vertical velocities against the normalized flow depth (z/h) in the developing and the developed flow regions, where z is the distance from the bed of the measurement point. Velocity distributions, displayed in Figure 2, showed that the position of maximum velocity in the streamwise direction shifted upward, indicating the growth in the boundary layer thickness along the developing region [20,21]. The data of the experimental runs E1 and E2 did not overlap, but the velocity distributions were distinct for the developing and developed flows. In the case of the no-seepage runs (i.e., runs E1 and E2), the mean velocity of the streamwise and vertical directions for the developing flow fulfilled its maximum value in the vicinity of the water surface and slowly decreased towards the channel boundary because of the flow resistance due to the bed roughness. In the condition of the developing flows, the velocity values in the streamwise and vertical directions were amplified in comparison to the developed flow. The flow depth was slightly lower in the developing zone, and gradually increased along the channel length until the fully-developed flow condition was achieved. As a consequence, the streamwise and vertical flow velocities were higher in the developing flow. Measurements revealed that the streamwise velocities close to the channel boundary increased by approximately 7–9% in the developing flow, and the vertical velocities increased by approximately 10–12%. The streamwise and vertical velocity profiles for developing turbulent boundary layers are in line with the available literature [10,21]. In the seepage experiments, velocity measurements through ADV were taken immediately after the application of seepage to understand the effects of downward seepage on the flow characteristics of the channel. Flow velocities in both the developing and developed flows were higher than in the no-seepage conditions. Similar to the no-seepage conditions, in the developing flow, the streamwise velocities close to the channel bed increased by approximately 6–8%, and the vertical velocities increased by approximately 9–12%, in comparison to the developed flow. The velocity defect in the outer zone was more in the developing flow condition, as compared to the developed flows. It was observed that seepage flow influenced the vertical velocities (w) more than those of the streamwise velocities (u). The observed data nearly overlapped for the streamwise velocity, whereas the experimental data were far apart in the case of the vertical velocity, indicating a higher level of turbulence with seepage. The existing literature in the application of downward seepage shows that the distribution of the velocity tends to move vertically downward and, therefore, a greater velocity is observed close to the channel boundary [22].

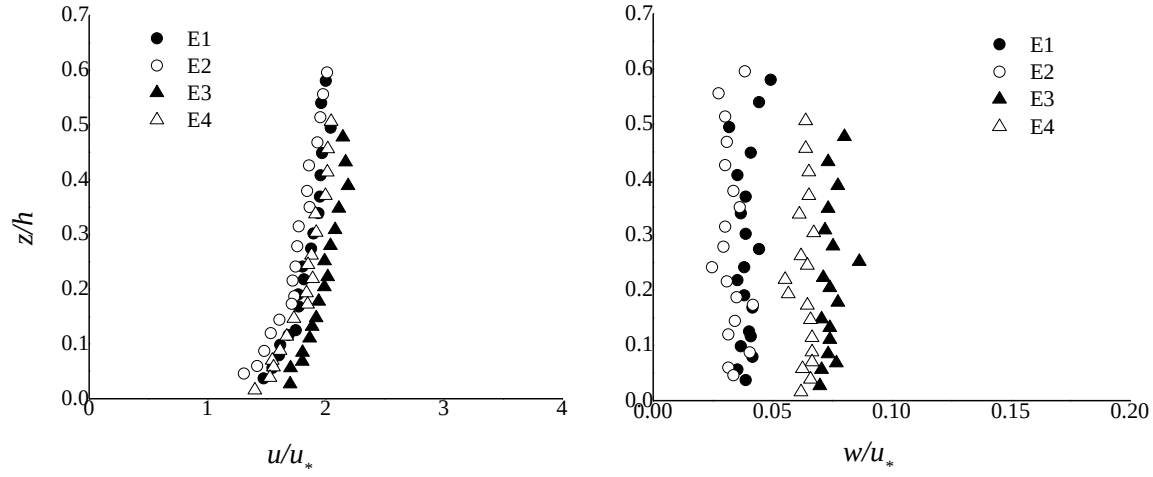

Figure 2. Vertical distribution of streamwise (u) and vertical (w) velocities for runs **E1** (developing flow and no-seepage), **E2** (fully-developed flow and no-seepage), **E3** (developing flow and downward seepage), and **E4** (fully-developed flow and downward seepage).

3.2. Reynolds Shear Stresses (RSSs)

The momentum exchange between the fluid structure and the bed material in the channel is called Reynolds shear stress. Hence, the RSS is a key factor that leads to sediment transport and erosion in the channel. The distributions of RSSs along the flow depth for the developing and developed flows over the no-seepage and downward seepage beds are presented in Figure 3. It was observed that RSS increased towards the bed, which is related to the momentum delivered from the fluid structures to the channel boundary, thus promoting sediment transport and overcoming the resistance of the grain. This observation is in agreement with previous studies [20,23]. The RSS achieved a peak magnitude in the inner layer of flow, and it reduced close to the channel boundary due to the roughness sub-layer. Figure 3 shows similar data trends for the RSS distributions in the developing and developed flows, but with different magnitudes. The greater magnitudes of RSS were found for the developed flow in comparison with the developing flow. This would imply the presence of a higher momentum exchange in developed flows. In addition, the upward decreasing trend of RSS would indicate that the farther the measurement point is from the channel boundary, the lower the turbulence generated by the flow in the developing and developed regions is. Hence, the distributions of RSS were evaluated to describe the momentum diffusion phenomena. A significant finding was that the peak value of RSS in the developed flow was higher than that in the developing flow by approximately 22.4% and 6.7% for the no-seepage and downward seepage conditions, respectively. In all the distributions, amplified values of RSSs were observed for runs in which downward seepage processes occurred. This would imply a greater momentum exchange near the bed, thus increasing the sediment mobility in the channel. In addition, a substantial increase in the RSS values were ascertained in the developed flows, resulting in higher velocity fluctuations in comparison with the developing flow. RSS indicated the turbulent intensities in the flow, as it was dependent on the velocity fluctuations.

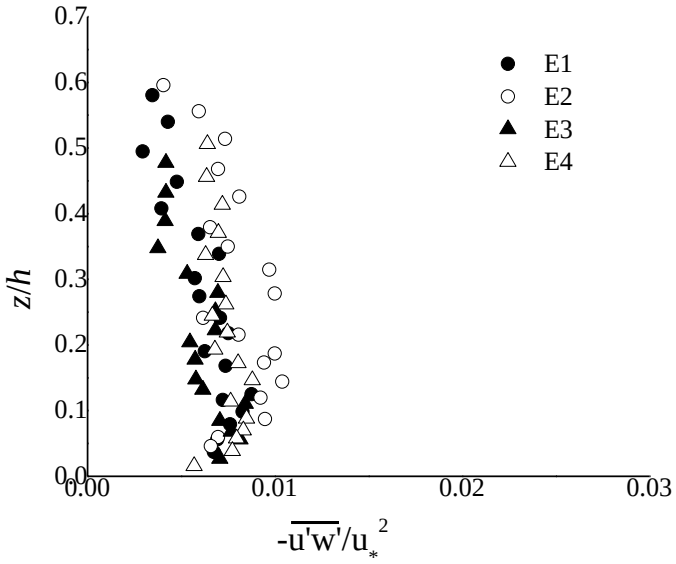

Figure 3. Depth profile of the Reynolds shear stress for runs **E1** (developing flow and no-seepage), **E2** (fully-developed flow and no-seepage), **E3** (developing flow and downward seepage), and **E4** (fully-developed flow and downward seepage).

3.3. Turbulence Intensities and Turbulence Kinetic Energy (TKE)

The turbulence intensity is an outcome of the variation in the instantaneous velocity at a measurement point determined by the velocity measurement and the type of bed roughness. Additionally, the root mean square (rms) of the fluctuating component of the

velocity indicates the turbulence intensities. Hence, the streamwise and vertical turbulence intensities represented by σ_u, and σ_w, respectively, are given by

$$\sigma_u = \sqrt{\frac{\sum_{i=1}^{n} (U_i - u)^2}{n}} \quad (1)$$

$$\sigma_w = \sqrt{\frac{\sum_{i=1}^{n} (W_i - w)^2}{n}} \quad (2)$$

where n is the number of samples, U_i and W_i represent the instantaneous velocities in the streamwise and vertical directions, respectively, and u and w represent the mean streamwise and vertical velocity components, respectively. The distributions along the flow depth of the turbulence intensities for the developing and developed flows are presented in Figure 4. The peak value for turbulence intensity was attained in the inner flow layer in both the developing and developed flows, where the maximum value of RSS was also observed with a tendency towards a steady condition. Close to the free surface, the turbulence intensities tended towards stationary values. Fluctuations in values were more pronounced near the channel boundary than in the region close to the water surface, due to the bed roughness. In addition, the degree of the turbulence intensity was higher in the developed flows than in the developing flows. A significant finding was that the near-bed streamwise turbulence intensities (σ_u) in the developed flow were higher by 10–30% than those in the developing flows over the seepage bed, whereas the increasing magnitude for the near-bed vertical turbulence intensities (σ_w) was 5–10%. The downward seepage in the channel escalated the flow velocity fluctuations in the near-bed region, with an increase in the flow turbulence near the bed. It was also observed that the distributions of the turbulence intensities over the seepage bed were higher in near-bed region, though slightly, compared to those in the case of the no-seepage bed condition. This result is in line with the existing literature [24,25].

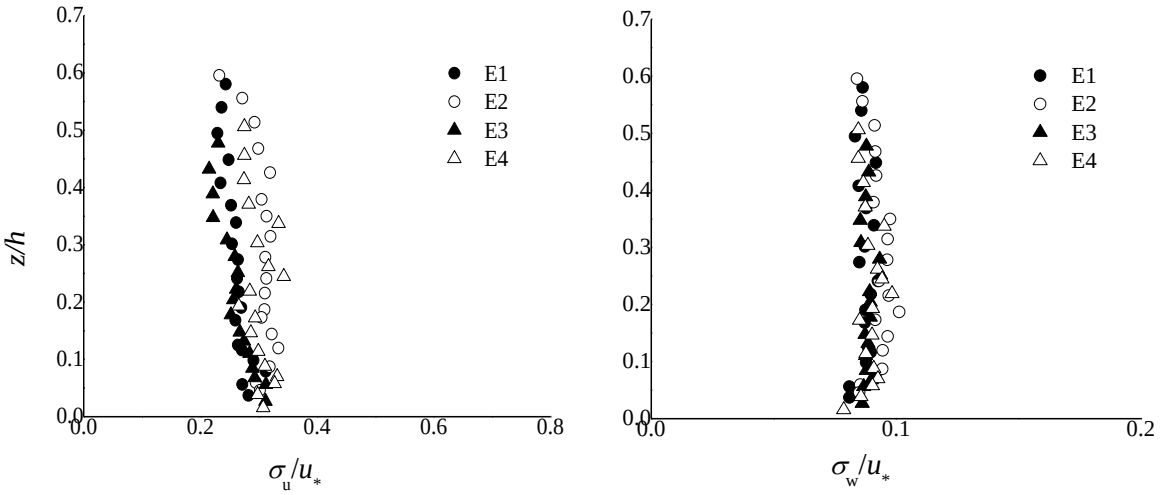

Figure 4. Vertical distribution of streamwise and vertical turbulence intensity for runs **E1** (developing flow and no-seepage), **E2** (fully-developed flow and no-seepage), **E3** (developing flow and downward seepage), and **E4** (fully-developed flow and downward seepage).

The normalized form of the streamwise (σ_u) and vertical (σ_w) turbulence intensities are represented by $\widehat{\sigma}_u = \sigma_u / u_*$ and $\widehat{\sigma}_w = \sigma_w / u_*$, where u_* is the shear velocity. An effort was made to revise the literature equations proposed for wide-open-channel flows. Numerous models were recommended to predict the distributions of the turbulence intensities and the flow depths in wide channels [1,6,17,20,26,27]. The existing literature models have not

considered the developing flow over the seepage bed, and the trends for the streamwise and vertical turbulence intensities in the developing and developed flows for the seepage experiments presented in Figures 5 and 6 do not match the universal models provided by previous studies. A regression study was performed to develop new empirical equations for flows in the developing and developed zones for no-seepage and downward seepage conditions. The functional forms of the semi-empirical expressions suggested in the literature [20,26] is considered in the present work, as shown below:

$$\left.\begin{array}{l} \frac{\sigma_u}{u_*} = \alpha_1 \exp\left(-\beta_1 \frac{z}{h}\right) \\ \frac{\sigma_w}{u_*} = \alpha_2 \exp\left(-\beta_2 \frac{z}{h}\right) \end{array}\right\} \text{developing flow}$$
$$\left.\begin{array}{l} \frac{\sigma_u}{u_*} = \alpha_3 \exp\left(-\beta_3 \frac{z}{h}\right) \\ \frac{\sigma_w}{u_*} = \alpha_4 \exp\left(-\beta_4 \frac{z}{h}\right) \end{array}\right\} \text{developed flow} \quad (3)$$

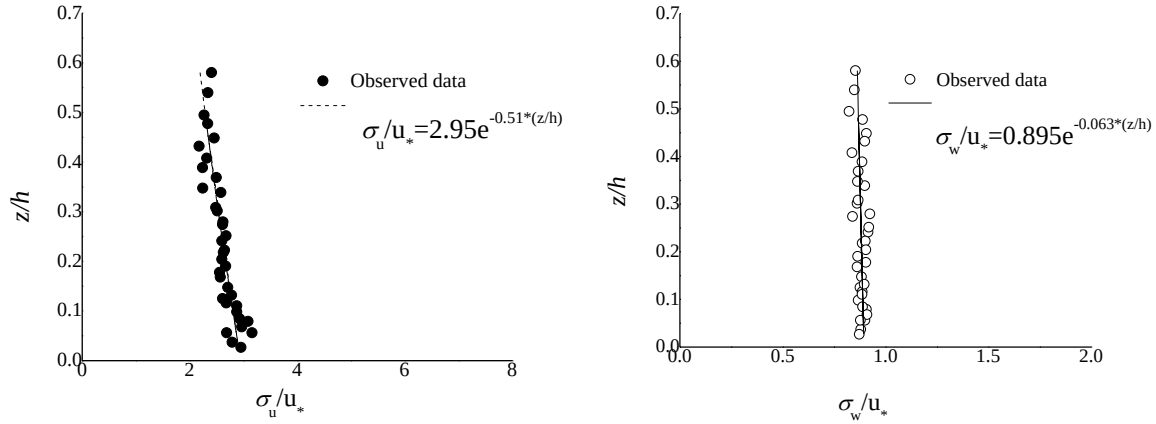

Figure 5. Vertical distributions of normalized streamwise and vertical turbulence intensities in developing flow.

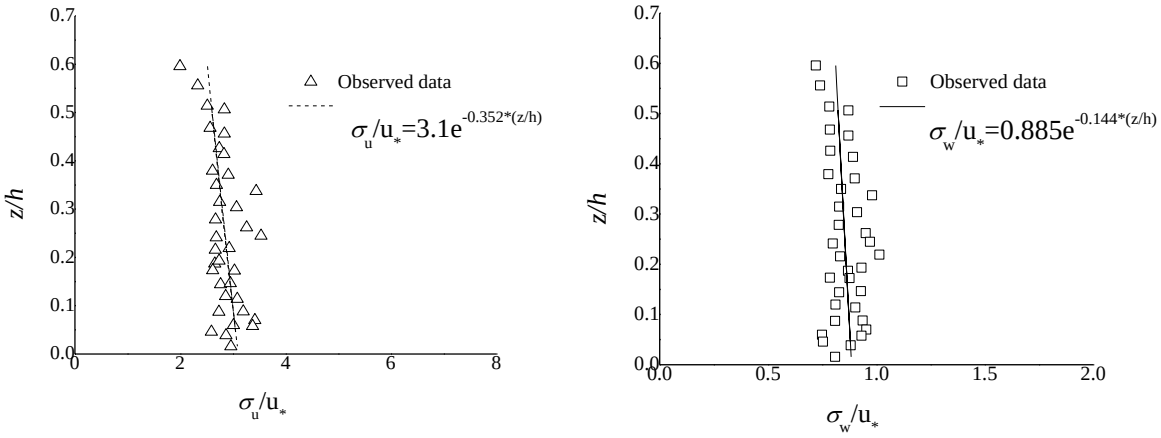

Figure 6. Vertical distributions of normalized streamwise and vertical turbulence intensities in developed flow.

In the above equations, the coefficients α_1, α_2, α_3, and α_4, and the exponential coefficients β_1, β_2, β_3, and β_4 were found from the data collected in this study. In particular, a regression study was performed. The current work revealed a modification in the magnitude of the coefficient and the exponential values from existing studies. The coefficients suggested here, as well as those from the existing literature are given in Table 2. The proposed empirical expressions are also displayed in Figures 5 and 6. The previous studies [20,28] remarked that the coefficient (α_3) of the streamwise turbulent intensities equation was greater than that (α_4) for the vertical turbulence intensities, i.e., $\alpha_3 > \alpha_4$; the same result was also found in the current work, as shown in Table 2. The velocity fluctuations in

the streamwise direction would increase the streamwise turbulence intensities, whereas the water surface was prone to decrease the vertical turbulence intensity in the vertical direction. The evaluation of the coefficients in the current work, and those from previous studies for smooth and rough beds, highlighted that the coefficient for the developed flows over the seepage bed was higher, indicating that the turbulence intensity profiles, in the case of seepage, were altered in comparison with those for wide-open-channel flows.

Table 2. Values of the coefficients observed from turbulent intensity equations.

Literature	α_1	α_2	α_3	α_4	β_1	β_2	β_3	β_4	Bed Characteristics
Present study	2.95	0.895	3.1	0.88	0.51	0.063	0.352	0.144	Hydraulically rough and seepage bed
Cardoso et al. [6]	-	-	2.28	-	-	-	1.08	-	Hydraulically smooth
Kironoto and Graf [17]	-	-	2.04	1.14	-	-	0.97	0.76	Hydraulically rough
Nezu and Azuma [26]	-	-	2.30	1.27	-	-	1	1	Hydraulically smooth and rough
Nezu and Nakagawa [20]	-	-	2.30	1.27	-	-	1	1	Hydraulically smooth and rough
Nezu and Rodi [27]	-	-	2.26	1.23	-	-	1	1	Hydraulically smooth and rough
Mahananda et al. [1]	-	-	2.52	1.35	-	-	1	1	Hydraulically rough and narrow open-channel flow

In addition, the distributions, along with the flow depth of the turbulent kinetic energy (TKE), $K_{2D} = 0.75\left(\overline{u'^2} + \overline{w'^2}\right)$ for the developing and developed flows, and in the cases of the no-seepage and downward seepage conditions, are displayed in Figure 7. It can be noted that for the developing and developed flows, the distributions did not overlap in both the no-seepage and downward seepage conditions. For a given flow discharge, the seepage run exhibited a greater mean TKE in the vicinity of the bed surface than the no-seepage run. A greater magnitude of TKE in the vicinity of the bed surface was observed for the developed flows due to the greater streamwise and vertical turbulence intensities [10]. As in the case of the fully-developed flows, the distribution of TKE in the developing flows showed the highest magnitude close to the channel boundary, and reduced quickly in the outer flow region. Finally, the vertical profiles of TKE for a given flow discharge were amplified for the developed flow, in comparison with the developing flows.

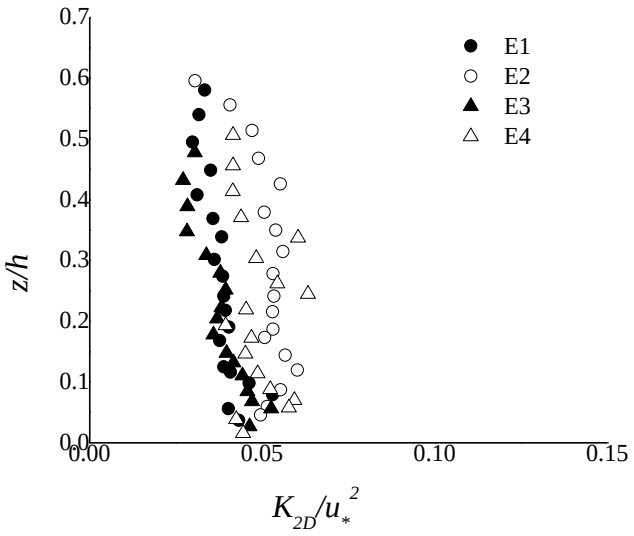

Figure 7. Vertical distribution of TKE for runs **E1** (developing flow and no-seepage), **E2** (fully-developed flow and no-seepage), **E3** (developing flow and downward seepage), and **E4** (fully-developed flow and downward seepage).

3.4. Fluctuating Velocities

Lu and Willmarth [29] developed the quadrant analysis to examine the presence of a coherent structure and to compute the input of coherent eddies into the production of Reynolds shear stresses. In this study, the velocity fluctuations in the four quadrants were explored in the flow's inner layer for the developing and developed flows to examine the comparative role of bursting events in producing turbulent shear stresses. In the quadrant analysis, streamwise u′ and vertical w′ fluctuating velocities were distributed into four quadrants on a u′-w′ plane. Each quadrant represented a type of bursting event, which occurred in the flow zone. The first quadrant represented outward interactions (u′ > 0, w′ > 0), which specified the outward transport of the high-speed fluid parcels. The second quadrant represented the ejections events (u′ < 0, w′ > 0), which implied the drive away of the low-speed fluid parcel from the channel boundary. Inward interactions (u′ < 0, w′ < 0), which defined low-speed fluid parcel motion towards the channel boundary, were signified by the third quadrant. The fourth quadrant (u′ > 0, w′ < 0) characterized sweep events defined by high-speed fluid parcel movement towards the channel bed. For the quadrant analysis, the position $z = 0.05h$ in the inner region was selected as a measurement point for the developing and developed flows for all experimental runs. For the developing flow, Figure 8 shows the scatter variations of the fluctuating velocities u′ and w′ for a hole size $H = 0$ in the case of no seepage (the diagram on the left) and downward seepage (the diagram on the right), respectively. The hole size $H = 0$ indicated the high frequency events, including the small values associated with the use of all the pairs of u′ and w′. By comparing the scatter plots for hole size $H = 0$, it was found that the level of the bursting events increased in the developed flow zone for the no-seepage and seepage conditions. A further important observation was that more events took place in the second and fourth quadrants in the vicinity of bed surface ($z = 0.05h$), showing that the sweep and ejection events were prone to govern the flow. These results are in line with the observations made by Bomminayuni and Stoesser [30]. From the comparison of the two data plots, it can be observed that the levels of the bursting events were stronger for the developing flows in the presence of downward seepage. With seepage, in the case of the developing flow, the average contributions from ejections and sweeps are increased by 28.6% and 24.5%, respectively, in comparison to the no seepage value.

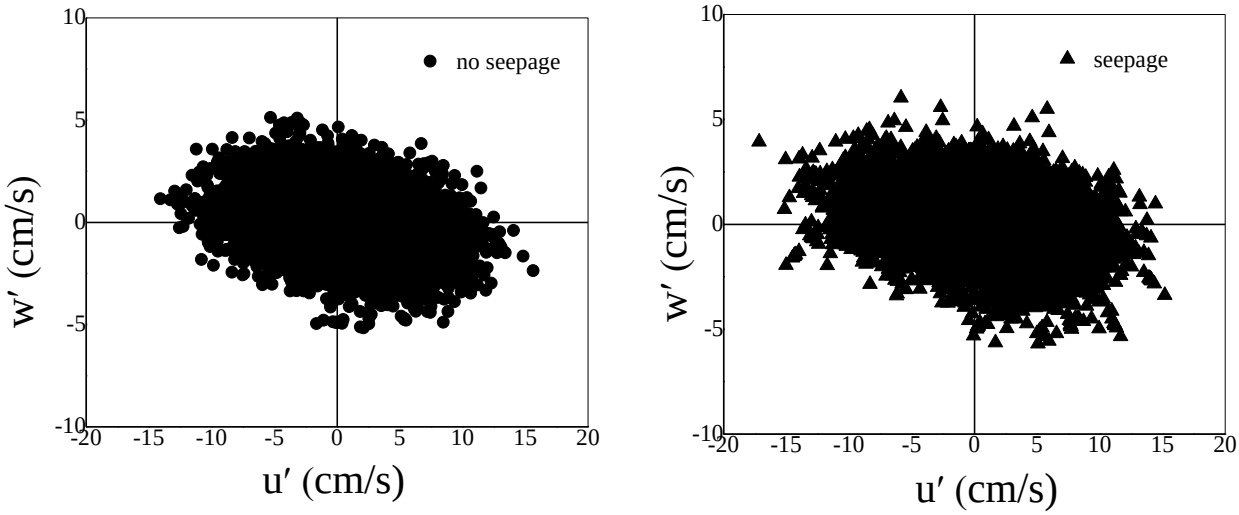

Figure 8. u′-w′ scatter plots with hole size $H = 0$ at selected point $0.05h$ in the developing flow region.

Figure 9 shows the scatter variations in the streamwise u′ and vertical w′ fluctuating velocities for hole size $H = 0$ in the inner regions of the developed flow, in the cases of the no-seepage and downward seepage experiments. The hole size $H = 0$ indicated that all u′ and w′ velocities were considered at the measurement point ($z = 0.05h$). Figure 9 shows that the sweep and ejection events mainly characterized the bursting events in the inner regions for

the no-seepage and downward seepage conditions, while the contribution of the outward and inward interactions was somewhat weak, as compared to the sweeps and ejections through the entire flow depth. The comparison of the scatter variation of streamwise u′ and vertical w′ showed that the degree of the bursting events was higher in second and fourth quadrants (ejection and sweep). In the no-seepage and downward seepage conditions, the plot area of the velocity fluctuations in the inner region was nearly eclipsed, which showed that the turbulence was highly anisotropic. The degree of turbulence fluctuations without normalization increased with seepage, as can be seen in Figure 9. The input of bursting events to the production of Reynolds stress, as a measurement point, can be expressed as [20]

$$\langle u\prime w\prime \rangle_{i,H} = \lim_{T\to\infty} \frac{1}{T} \int_0^T u\prime(t) w\prime(t) I_{i,H}[u\prime(t) w\prime(t)] \mathrm{dt} \quad (4)$$

where t, T, and $I_{i,H}$ signify the time, sampling duration, and the indicator function, respectively. The indicator function is expressed as

$$I_{i,H}[u'(t)w'(t)] = \begin{cases} 1, \text{ if } (u', w') \text{is in quadrant } i \text{ and if } |u'w'| \geq H\left(\overline{u'^2}\right)^{0.5}\left(\overline{w'^2}\right)^{0.5} \\ 0, \text{ otherwise} \end{cases} \quad (5)$$

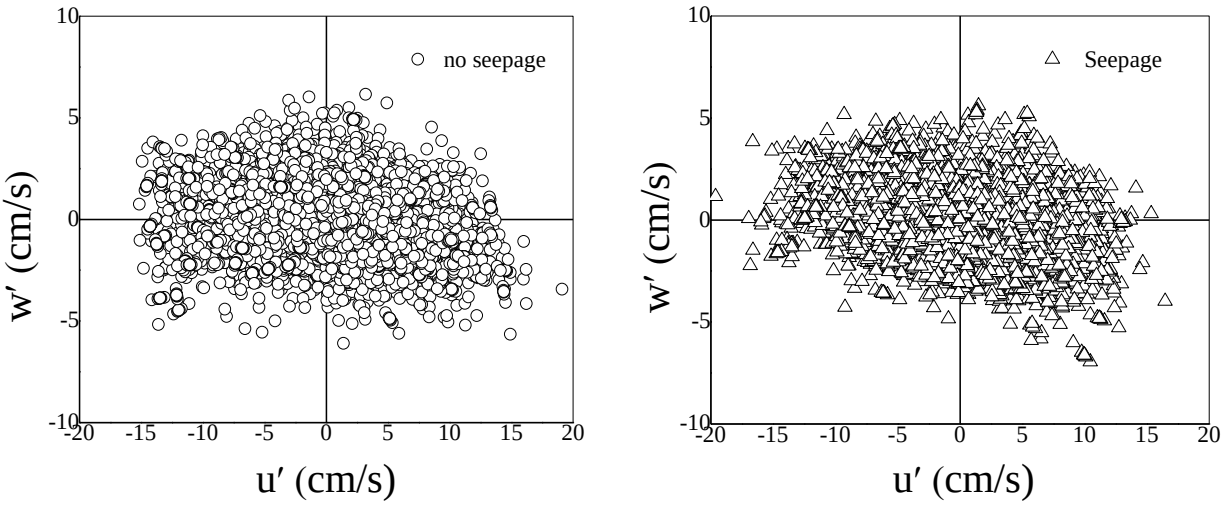

Figure 9. u′-w′ scatter plots with hole size $H = 0$ at a depth $z = 0.05h$ in fully-developed flow region.

A greater number of events occurred in the second and fourth quadrants, describing the ejections and sweeps, which governed the flow. With seepage, in the case of developed flow, the average contributions from ejections and sweeps were increased by 13.6% and 3.5%, respectively, in comparison to the no-seepage condition. From Figures 8 and 9, and for a given flow discharge, the developed flow over the seepage bed had the maximum fluctuations, while the developing flow with the no-seepage bed was characterized by the lowest fluctuations.

3.5. Turbulent Correlation Coefficient

Figure 10 presents the depth profiles of the correlation coefficient $r_{uw} = \left[-\overline{u'w'}/\sigma_u\sigma_w\right]$ (at different water heights) for the developing and fully-developed flows with no-seepage and downward seepage conditions. It was observed that the correlation coefficient for the fully-developed flow was typically higher than that of the developing flow throughout the flow depth. The change in the correlation coefficient for the fully-developed flow was due to the relative modification of the Reynolds shear stress over the turbulence intensity. Figure 10 also reveals that the correlation coefficient reduces, although very gradually, in the vicinity of the bed surface for both the developing and fully-developed flows. Interestingly,

this observation matches the findings of Kironoto and Graf [31] for hydraulically rough wide-channels. The effect of seepage on the correlation coefficient was noticeable, as the correlation coefficient near the bed for the seepage runs was generally lower, by 5–10%, than in the case of the no-seepage condition. The observed correlation coefficient changes over the seepage bed were due to the comparative alteration of the Reynolds shear stresses over the turbulence intensities.

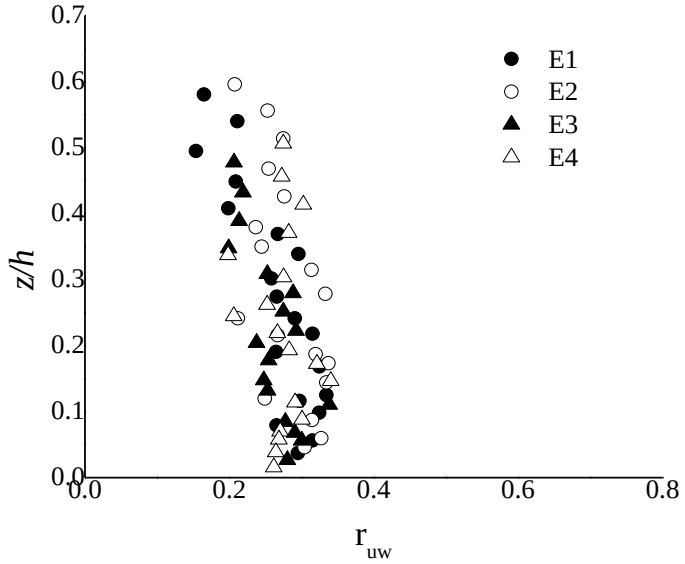

Figure 10. Vertical distribution of the correlation coefficient r_{uw} (i.e., the ratio of the Reynolds shear stress to the product of turbulence intensities in streamwise and vertical directions) for runs **E1** (developing flow and no-seepage), **E2** (fully-developed flow and no-seepage), **E3** (developing flow and downward seepage), and **E4** (fully-developed flow and downward seepage).

3.6. Reynolds Stress Anisotropy Tensor

Reynolds stress anisotropy proposed the approximation for the level of deviation from the isotropy in order to calculate the anisotropy in a turbulent flow. Therefore, the fluctuating components of velocities were used to evaluate the anisotropy tensor of the Reynolds shear stress, which further illustrated that the flow was anisotropic in nature. The Reynolds stress anisotropy tensor b_{ij} was expressed as the ratio of the Reynolds stress parameter to the turbulence kinetic energy, minus its isotropic equivalent magnitude. Reynolds stress anisotropy is an estimate of the deviation from isotropic turbulence ($b_{ij} = 0$). Thus, b_{ij} is calculated as $b_{ij} = \frac{\overline{u_i' u_j'}}{2K} - \frac{\delta_{ij}}{3}$ where $K = \frac{1}{2}\left(\overline{u'u'} + \overline{v'v'} + \overline{w'w'}\right)$ represents the turbulent kinetic energy, and δ_{ij} denotes the Kronecker delta function, defined by δ_{ij} $(i \neq j) = 0$ and δ_{ij} $(i = j) = 1$. From a physical point of view, the anisotropy tensor components b_{11}, b_{22}, and b_{33} can be regarded as the relative contributions of the turbulence intensities in streamwise, spanwise, and vertical directions to the average turbulent kinetic energy. On the other hand, the component b_{13} signifies the ratio of the Reynolds shear stress to the average turbulent kinetic energy value. The anisotropy parameters b_{11}, b_{12}, b_{22}, and b_{33} are plotted in Figure 11. The parameter b_{ij} is a symmetric and traceless tensor, given as $1/3 \leq b_{ij} \leq 2/3$, and b_{ij} disappears in isotropic turbulence. The symbol of each diagonal variable in b_{ij} signifies the respective input of the turbulence intensity parameters, compared with the turbulent kinetic energy. Figure 11 shows the changes in the stress anisotropy tensors b_{ij} with a non-dimensional flow depth z/h for the developing and developed flows, where z represents the vertical distance taken from the bed surface, as mentioned above. The profile of the anisotropy tensor component b_{11} for the developing flow implied the higher anisotropic stream at the near-bed region in the flow direction in comparison to that of b_{11} for developed flow, whereas b_{13}, b_{22}, and b_{33} in the vicinity of the bed level for developing flow provided the lower anisotropic stream in comparison to those of b_{13}, b_{22},

and b_{33} of the developed flow. Papanicolaou et al. [32] also observed that the features of bed morphology influenced the fluid Reynolds stresses; therefore, the current results are in good agreement with the existing literature. Further, the anisotropy parameters b_{13}, b_{22}, and b_{33} can be considered the comparative influence of the turbulence intensities in streamwise, spanwise, and vertical directions on the average turbulent kinetic energy.

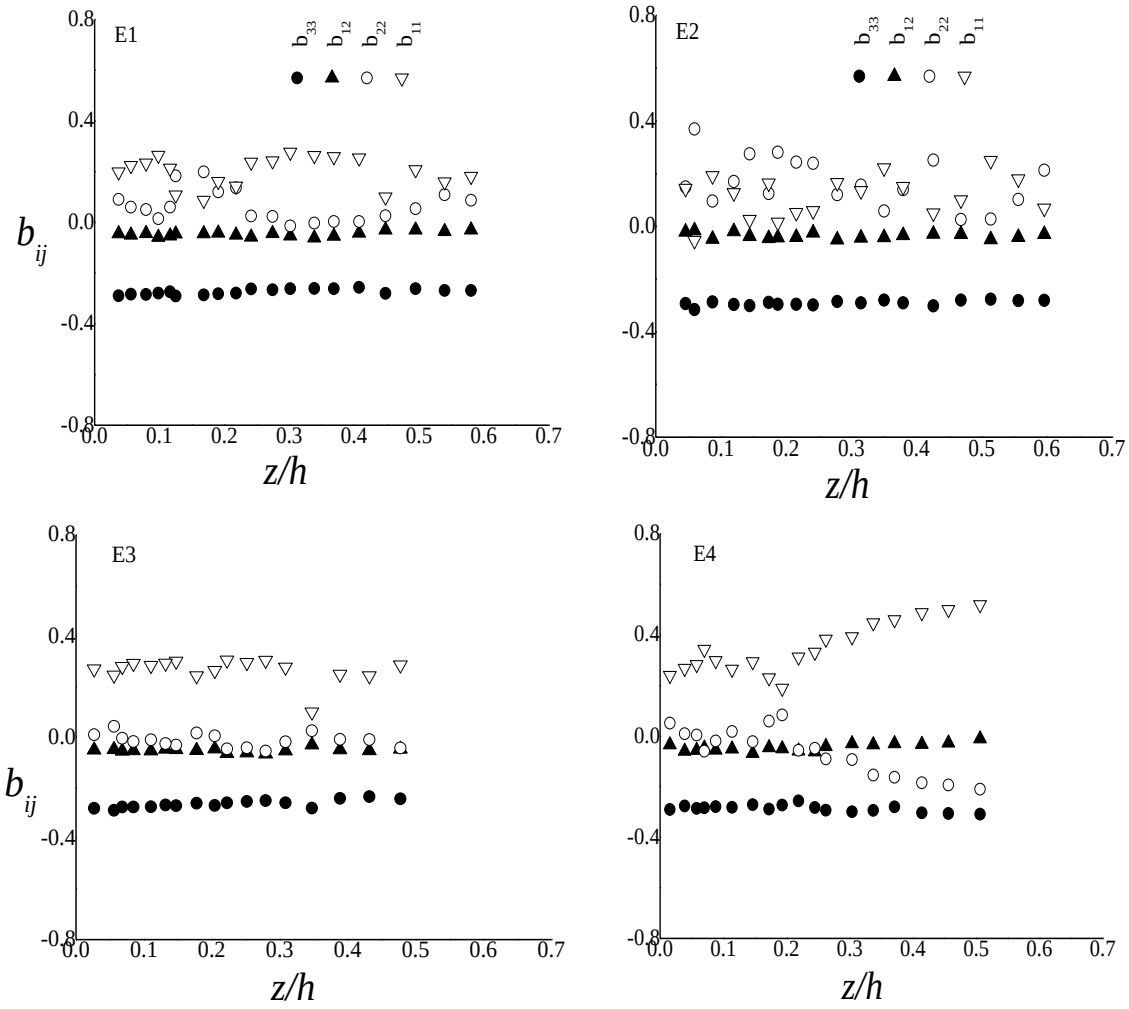

Figure 11. Reynolds stress anisotropy tensor (b_{33}, b_{12}, b_{22} and b_{11}) for runs **E1** (developing flow and no-seepage), **E2** (fully-developed flow and no-seepage), **E3** (developing flow and downward seepage), and **E4** (fully-developed flow and downward seepage).

4. Conclusions

The fluid structures in the developing and developed wide-open-channel flows over a sandy bed were investigated in the present work. A series of experiments were carried out in a laboratory flume to investigate the fluid features of downward seepage. The streamwise and vertical velocity variations in the developing flow were found to be higher than that in the developed flow. Similar profiles were observed in the no-seepage and downward seepage conditions, but streamwise and vertical velocities increased under the influence of seepage. The Reynolds shear stress (RSS) distributions were lightly scattered and increased in the developed flow, implying a larger momentum transfer from the flow to the channel bed. Similar distributions were found in the no-seepage and seepage runs, where RSS also increased under the effect of seepage. The profiles of the RSS follow the damping trends in the vicinity of the channel boundary because of the decreased velocity fluctuations near the channel bed. In the developed flow region, the streamwise and vertical turbulence intensities were found to be amplified compared to the developing flow. New

exponential expressions were developed for turbulence intensities in the developing and developed flows over the seepage bed. The streamwise anisotropy tensor in the developing flow depicts the higher values of an anisotropic stream in the vicinity of the bed surface, compared to the developed flow. The quadrant analysis results signified that the level of instantaneous velocity fluctuations, without normalization, increased in the developed flow for a given flow discharge. Further, the instantaneous velocity fluctuations in the developing flow decreased in the no seepage and downward seepage conditions. For all experimental runs, the turbulent correlation coefficient increased in the developed flow.

Author Contributions: For conceptualization, A.S.; methodology, A.S. and B.K.; formal analysis, A.S. and B.K.; investigation, A.S. and B.K.; writing—original draft preparation, A.S.; writing—review and editing, A.S., B.K. and G.O.; visualization, G.O. All authors have read and agreed to the published version of the manuscript.

Funding: This research received no external funding.

Institutional Review Board Statement: Not applicable.

Informed Consent Statement: Not applicable.

Data Availability Statement: The data presented in this study are available on request from the corresponding author.

Conflicts of Interest: The authors declare no conflict of interest.

References

1. Mahananda, M.; Hanmaiahgari, P.R.; Balachandar, R. Effect of aspect ratio on developing and developed narrow open channel flow with rough bed. *Can. J. Civ. Eng.* **2018**, *45*, 780–794. [CrossRef]
2. Kirkgöz, M.S.; Ardiçlioğlu, M. Velocity profiles of developing and developed open channel flow. *J. Hydraul. Eng.* **1997**, *123*, 1099–1105. [CrossRef]
3. Sharma, A.; Kumar, B. Boundary layer development over non-uniform sand rough bed channel. *ISH J. Hydraul. Eng.* **2019**, *25*, 162–169. [CrossRef]
4. Maclean, A.G. Open channel velocity profiles over a zone of rapid infiltration. *J. Hydraul. Res.* **1991**, *29*, 15–27. [CrossRef]
5. Shahiri Tabarestani, E.; Afzalimehr, H.; Pham, Q.B. Validation of double averaged velocity method in a variable width river. *Earth Sci. Inform.* **2021**, *14*, 2265–2278. [CrossRef]
6. Tominaga, A.; Nezu, L. Velocity profiles in steep open-channel flows. *J. Hydraul. Eng.* **1992**, *118*, 73–90. [CrossRef]
7. Cardoso, A.H.; Graf, W.H.; Gust, G. Uniform flow in a smooth open channel. *J. Hydraul. Res.* **1989**, *27*, 603–616. [CrossRef]
8. Xinyu, L.; Changzhi, C.; Zengnan, D. Turbulent flows in smooth-wall open channels with different slope. *J. Hydraul. Res.* **1995**, *33*, 333–347. [CrossRef]
9. Coles, D. The law of the wake in the turbulent boundary layer. *J. Fluid Mech.* **1956**, *1*, 191–226. [CrossRef]
10. Mahananda, M.; Hanmaiahgari, P.R.; Balachandar, R. On the turbulence characteristics in developed and developing rough narrow open-channel flow. *J. Hydro Environ. Res.* **2021**, *40*, 17–27. [CrossRef]
11. Han, Y.; Yang, S.-Q.; Sivakumar, M.; Qiu, L.-C. Investigation of velocity distribution in open channel flows based on conditional average of turbulent structures. *Math. Probl. Eng.* **2017**, *2017*, 1458591. [CrossRef]
12. Marusic, I.; McKeon, B.J.; Monkewitz, P.A.; Nagib, H.M.; Smits, A.J.; Sreenivasan, K.R. Wall-bounded turbulent flows at high Reynolds numbers: Recent advances and key issues. *Phys. Fluids* **2010**, *22*, 065103. [CrossRef]
13. Rao, A.R.; Sreenivasulu, G.; Kumar, B. Geometry of sand-bed channels with seepage. *Geomorphology* **2011**, *128*, 171–177. [CrossRef]
14. Sharma, A.; Kumar, B. Structure of turbulence over non uniform sand bed channel with downward seepage. *Eur. J. Mech. B Fluid.* **2017**, *65*, 530–551. [CrossRef]
15. Liu, Y.; Wallace, C.D.; Zhou, Y.; Ershadnia, R.; Behzadi, F.; Dwivedi, D.; Xue, L.; Soltanian, M.R. Influence of streambed heterogeneity on hyporheic flow and sorptive solute transport. *Water* **2020**, *12*, 1547. [CrossRef]
16. ANCID. *Australian Irrigation Water Provider Benchmarking Data Report for 2004–2005*; Australian National Committee on Irrigation and Drainage: Canberra, Australia, 2006.
17. Tanji, K.K.; Kielen, N.C. *Agricultural Drainage Water Management in Arid and Semi-Arid Areas*; FAO Irrigation and Drainage Paper 61, Publishing Management Service, Information Division; FAO: Rome, Italy, 2002.
18. Sharma, A.; Maddirala, A.K.; Kumar, B. Modified singular spectrum analysis for despiking acoustic Doppler velocimeter (ADV) data. *Meas. J. Int. Meas. Confed.* **2018**, *117*, 339–346. [CrossRef]
19. Martin, C.A.; Gates, T.K. Uncertainty of canal seepage losses estimated using flowing water balance with acoustic Doppler devices. *J. Hydrol.* **2014**, *517*, 746–761. [CrossRef]
20. Nezu, I.; Nakagawa, H. *Turbulence in Open-Channel Flows*; IAHR Monograph, A.A. Balkema: Rotterdam, The Netherlands, 1993.

21. Lane, S.N.; Biron, P.M.; Bradbrook, K.F.; Butler, J.B.; Chandler, J.H.; Crowell, M.D.; Roy, A.G. Three-dimensional measurement of river channel flow processes using acoustic Doppler velocimetry. *Earth Surf. Process. Landf.* **1998**, *23*, 1247–1267. [CrossRef]
22. Cao, D.; Chiew, Y.M. Suction effects on sediment transport in closed conduit flows. *J. Hydraul. Eng.* **2014**, *140*, 04014008. [CrossRef]
23. Bonakdari, H.; Lipeme-Kouyi, G.; Asawa, G.L. Developing turbulent flows in rectangular channels: A parametric study. *J. Appl. Res. Water Wastewater* **2014**, *1*, 51–56.
24. Faruque, M.A.A.; Balachandar, R. Seepage effects on turbulence characteristics in an open channel flow. *Can. J. Civ. Eng.* **2011**, *38*, 785–799.
25. Lu, Y.; Chiew, Y.M.; Cheng, N.S. Review of seepage effects on turbulent open-channel flow and sediment entrainment. *J. Hydraul. Res.* **2008**, *46*, 476–488. [CrossRef]
26. Nezu, I.; Azuma, R. Turbulence characteristics and interaction between particles and fluid in particle-laden open channel flows. *J. Hydraul. Eng.* **2004**, *130*, 988–1001. [CrossRef]
27. Nezu, I.; Rodi, W. Open-channel flow measurements with a Laser Doppler Anemometer. *J. Hydraul. Eng.* **1986**, *112*, 335–355. [CrossRef]
28. Papanicolaou, A.N.; Hilldale, R. Turbulence characteristics in gradual channel transition. *J. Eng. Mech.* **2002**, *128*, 948–960. [CrossRef]
29. Lu, S.S.; Willmarth, W.W. Measurements of the structure of the Reynolds stress in a turbulent boundary layer. *J. Fluid Mech.* **1973**, *60*, 481–511. [CrossRef]
30. Bomminayuni, S.; Stoesser, T. Turbulence statistics in an open-channel flow over a rough bed. *J. Hydraul. Eng.* **2011**, *137*, 1347–1358. [CrossRef]
31. Kironoto, B.A.; Graf, W.H. Turbulence characteristics in rough uniform open-channel flow. *Proc. Inst. Civ. Eng. Water Marit. Eng.* **1994**, *106*, 333–344. [CrossRef]
32. Papanicolaou, A.N.; Diplas, P.; Evaggelopoulos, N.; Fotopoulos, S. Stochastic incipient motion criterion for spheres under various bed packing conditions. *J. Hydraul. Eng.* **2002**, *128*, 369–380. [CrossRef]